Disponible en ligne sur
SciVerse ScienceDirect
www.sciencedirect.com

Elsevier Masson France
EM|consulte
www.em-consulte.com

IRBM

IRBM 33 (2012) 243–252

Original article

Comparing structural and functional graph theory features in the human brain using multimodal MRI

Comparaison des caractéristiques des graphes structurel et fonctionnel dans le cerveau humain à partir d'IRM

A. Messé [a,*,b,c,d], G. Marrelec [a,c,d], P. Bellec [c,d,e], V. Perlbarg [a,c,d], J. Doyon [c,d,e], M. Pélégrini-Issac [a,c,d], H. Benali [a,c,d,f]

[a] *Laboratoire d'imagerie fonctionnelle (LIF), UMR-S 678 Inserm/UPMC université Paris-6, CHU Pitié-Salpêtrière, 91, boulevard de l'Hôpital, 75634 Paris cedex 13, France*

[b] *Inria Sophia Antipolis – Méditerranée, Project Team Athena, 06902 Sophia Antipolis, France*

[c] *Laboratoire international de neuroimagerie et modélisation (LINeM), inserm, université de Montréal, 4565, chemin Queen-Mary, Montréal (Québec), H3W 1W5, Canada*

[d] *UPMC université Paris-6, 4, place Jussieu, 75005 Paris, France*

[e] *McConnell Brain Imaging Center, Montreal Neurological Institute, McGill University, Montréal, H3B 2B4, Canada*

[f] *Université de Montréal, MIC/UNF, Montréal, H3W 1W5, Canada*

Received 30 October 2011; received in revised form 18 February 2012; accepted 27 April 2012
Available online 7 September 2012

Abstract

Recent advances in magnetic resonance imaging (MRI) are allowing neuroscientists to gain critical insights into the neural networks mediating a variety of cognitive processes. This work investigates structural and functional connectivity in the human brain under different experimental conditions through multimodal MRI acquisitions. To define the nodes of a full-brain network, a set of regions was identified from resting-state functional MRI (fMRI) data using spatial independent component analysis (sICA) and a hierarchical clustering technique. Diffusion-weighted imaging (DWI) data were acquired from the same subjects and a probabilistic fiber tracking method was used to estimate the structure of this network. Using features originating from graph theory, such as small-world properties and network efficiency, we characterized the structural and functional connectivities of the full-brain network and we compared them quantitatively. We showed that structural and functional networks shared some properties in terms of topology as measured by the distribution of the node degrees, hence supporting the existence of an underlying anatomical substrate for functional networks.

1. Introduction

Large-scale neural networks are distributed by local neural assemblies transiently linked by long-distance reciprocal dynamic connections [1]. Such networks are thought to form an essential substrate for the performance of most cognitive functions. Uncovering how these networks operate is thus a key question to understand how the brain works [2,3]. Unfortunately, the structural and functional properties of human brain networks remain to be fully characterized. In particular, the focus of this paper is to understand how structure supports function.

Both structure and function can be indirectly imaged in vivo using magnetic resonance imaging (MRI). On one hand, diffusion-weighted imaging (DWI) provides significant insight into structural white matter pathways within the brain [4]. Tractography algorithms use DWI to reconstruct white matter fiber bundles, connecting distant brains regions, thereby granting access to structural connectivity networks [5,6]. On the other hand, functional MRI (fMRI) gives an indirect access to neuronal activity through its metabolic and hemodynamic consequences, using the blood oxygen level-dependent (BOLD) contrast [7,8]. Various approaches have relied on fMRI to identify sets of functionally dependent brain regions constituting functional

* Corresponding author.
E-mail address: Arnaud.Messe@imed.jussieu.fr (A. Messé).

1959-0318/$ – see front matter © 2012 Elsevier Masson SAS. All rights reserved.
http://dx.doi.org/10.1016/j.irbm.2012.04.005

connectivity networks. Such approaches have been applied to a wide range of experimental conditions and also at rest, i.e. while the subject lies still and refrains from any overt activity [9–13], see Perlbarg and Marrelec [14] for review.

In the recent years, complex networks have received a significant attention in scientific disciplines ranging from biology to economy and social sciences. Networks can be seen as graphs (a set of nodes linked by edges) and graph-theoretical methods have been applied to characterize their properties [15–19]. Most networks found in various fields are neither totally disordered (random) nor totally regular (lattice) but rather exhibit the so-called small-world properties [16,19,20]. Many recent studies of the literature rely on such graph-theoretical approach to investigate brain architecture using DWI and fMRI acquisitions [21–23].

This work is an original investigation of the structural and functional features of human brain networks using real multimodal MRI acquisitions (DWI and fMRI). Starting from a set of functional nodes identified from resting-state functional MRI data, we computed structural and functional (at rest, during motor task, and visual stimulation) connectivities between these nodes to define a network spanning the whole brain. We then examined the structural and functional connectivities of this network using measures drawn from graph theory, such as small-worldness or efficiency. Finally, we performed a quantitative statistical comparison of the network properties derived from structural and functional connectivities.

2. Materials and methods

2.1. Subjects

The present study included thirteen healthy right-handed volunteers (age 24–30, nine male) who were scanned at the Montreal Geriatric Institute, Montreal, Quebec, Canada, according to a protocol approved by the local ethic committee. The subjects had no history of neurological or psychiatric disorders. Functional data were recorded during three different conditions: a continuous rest period, during which subjects remained eyes closed, and two block-design paradigms: the first paradigm alternated between a motor and a control task, while the second alternated between a visual stimulation and a control task. For both motor and visual conditions, each epoch lasted for 30 s and was preceded by a 3-second visual instruction period. The motor task consisted of performing a left-hand finger-tapping movement paced at 2 Hz by a fixation cross-displayed on a screen. The visual stimulation consisted of an optic flow display, where white dots moving in a black background simulated the visual perception experienced during self-movement in a three-dimensional cloud; subjects were instructed to focus on a fixation cross located at the center of the screen. The control task lasted for 30 s and consisted of focusing on a fixation cross at the center of the screen.

2.2. Image acquisition and data preprocessing

Functional MRI series were recorded using a single-shot, gradient-recalled echo-planar imaging sequence (repetition time [TR]: 3500 ms; echo time [TE]: 40 ms; flip angle: 90°; matrix 64×64 voxels). One hundred and sixty T^{*2}-weighted images were acquired for each run. Each volume consisted of 41 contiguous axial slices (voxel size: 3.5 mm isotropic). Two runs were acquired in each experimental condition and for each subject. DWI data were recorded using a single-shot, echo-planar imaging sequence (TR: 8200 ms; TE: 97 ms; matrix 128×128 voxels). Twelve independent diffusion-weighted directions ($b = 1000\ s.mm^{-2}$) and a non-weighted image ($b = 0\ s.mm^{-2}$) were acquired four times for each subject and these repetitions were averaged. Each volume consisted of 52 contiguous axial slices (voxel size: 2 mm isotropic). A high-resolution co-planar anatomical volume (128 axial slices, voxel size: 1 mm isotropic) was also acquired during the same scanning session using a three-dimensional, spoiled gradient echo sequence (TR: 22 ms, TE: 4 ms, flip angle: 30°; matrix 256×256 voxels). All scans were performed on a 3T Siemens Magnetom Trio MRI scanner.

For each subject prior to data analysis, fMRI data were corrected for slice timing using the SPM2 software (Statistical Parametric Mapping: http://www.fil.ion.ucl.ac.uk/spm/software/spm2/). The resulting data were then corrected for quadratic drifts using linear regression. Volumes from the two runs corresponding to a same experimental condition were then concatenated. FMRI data were registered to the standard Montreal Neurological Institute (MNI) space using the nonlinearly approach of SPM2 and its EPI template [24]. Furthermore, each DWI scan was aligned to the non-weighted image (reference) using affine registration intended to maximise mutual information [25] and brain extraction derived from this reference scan was then applied to each volume [26] using the FSL software package (FMRIB Software Library, version 4.1: http://www.fmrib.ox.ac.uk/fsl/). The non-linear transformation of the non-weighted DWI scan of each subject to the MNI space was also computed using SPM2.

2.3. Constructing the full-brain network

2.3.1. Defining the regions of interest

We used spatial independent component analysis (sICA) to separate temporally and spatially structured brain processes at the group level [27,28]. The forty independent components that explained most variance were first extracted for each subject. We then clustered the spatial independent components into classes, which were representative of the population using a hierarchical clustering algorithm that maximizes within-class spatial similarity [29]. Spatial similarity was quantified using a distance d derived from the spatial correlation between components, as follows: $d_{ij} = \sqrt{1 - r_{ij}}$, where r_{ij} is the spatial correlation coefficient between component i and j. From the similarity tree, an *ad hoc* algorithm was used to define the group-representative components by optimizing both the degree of representativity (DR) and the degree of unicity (DU) of each group component. For a given class, DR was defined as the number of distinct runs that contributed to it, divided by the total number of runs. DU was defined as the number of runs that contributed to the class with one and only one component, divided by the number of distinct runs that contributed to it. The procedure selects

a group component if at least half of the runs contribute to it (DR > 0.5) and at least 75% of these runs contribute with only one component (DU > 0.75). Finally, for each class, we computed a fixed-effect group map of *t*-scores from all the individual spatial maps belonging to the class. All the group *t*-score maps were thresholded at $P < 0.05$ (not corrected for multiple comparisons) and visually inspected to select those that exhibited a spatial organization distributed into cortical, subcortical, and cerebellar areas known to be involved in cognitive, perceptual and sensorimotor functions; the other classes were related to noise processes (either physiological or physical) with known spatial distributions [30]. A set of regions of interest (ROIs) were finally semi-automatically defined from all selected maps by applying a region-growing algorithm (based on local covariance and 26-connexity) starting from local *t*-score maxima selected manually (the stopping criterion was a cluster size of 30 voxels). Each selected map could be considered as a distinct network, however each network only corresponded to roughly twenty ROIs, which was not large enough to derive graph-theoretical measures. As a consequence, the categorisation of selected nodes into functional networks was not taken into account, and the nodes from all networks were considered together to generate full-brain graph measures.

2.3.2. Indices of structural and functional connectivity

To quantify structural connectivity, ROIs were mapped back to each subject's diffusion space by applying the inverse transformation from the MNI space to the individual DWI space of each subject. A probabilistic white matter fiber tracking method [31] implemented in FSL was then used to track all possible connections between all pairs of ROIs. The fiber tracking parameters were: 5000 particles per voxel; 0.5 mm propagation step; maximal fiber curvature: 80°; no anisotropy constraint. An index of structural connectivity (sCI) between two ROIs was then defined as the fraction of samples connecting these two ROIs. This allowed to quantify the structural aspect of the global nework, which was eventually symmetrized by averaging forward and backward structural connectivites.

The functional connections were generated as follows. The time series of all voxels within a given ROI were spatially averaged to form the representative signal of that ROI. An index of functional connectivity (fCI) between two ROIs was then defined as the absolute correlation between the representative signals of these two ROIs for each of the three experimental conditions (fCIr at rest, fCIm during the motor task, and fCIv for the visual stimulation). This allowed us to quantify three functional states of the full-brain network. Each connectivity index (sCI, fCIr, fCIm, and fCIv) was finally displayed in a connectivity matrix for each subject.

2.4. Network characterization

The full-brain network was defined as the set of ROIs (or nodes, defined above) linked by connections (or edges, weighted by sCI, fCIr, fCIm, or fCIv), mathematically described as graphs. To quantify the topological organization of these graphs, we used several measures drawn from classical graph theory, including measures specifically developed for the analysis of small-world properties. These measures were used to compare quantitatively structural and functional features of the network. Computation of the graph-theoretical measures was carried out using a Matlab® (The Mathworks, Inc.) toolbox (Brain Connectivity Toolbox: http://www.brain-connectivity-toolbox.net/) described in detail in reference [23].

2.4.1. Small-world properties

We used small-world parameters derived from the characteristic path length of a network and its clustering coefficient [20]. The characteristic path length L of a network is the average length of the shortest path between all pairs of nodes, where the path length (also called distance) between two nodes corresponds to the minimum number of distinct edges required to link these nodes. The clustering coefficient C is the average of the clustering coefficients of all nodes, where the clustering coefficient of a node is the ratio between the actual number of edges among the node's neighbours and the largest number of possible connections within this neighbourhood. Random and lattice networks represent extremes of network topology from a totally disordered (random) network to a totally regular (lattice) network. Typically, a random network is characterized by small L and C values compared with a regular network. Small-world networks are located between the two extreme configurations and are characterized by a small L value (comparable to random networks) and a high C value (comparable to lattice networks). To measure the small-world properties of the structural and functional connectivity networks defined in the previous section, we scaled L (respectively, C) by dividing its value by the mean L (respectively, C) value obtained for 100 matched random networks (i.e. networks with the same size and density as the analyzed network); scaled L and C values were denoted by L_s and C_s, respectively [32,33]. A network will therefore be considered as having the small-world properties if it meets the following criteria: $L_s \approx 1$ and $C_s > 1$ [20].

2.4.2. Efficiency

Network efficiency is expressed in terms of global efficiency (E_g, related to the inverse characteristic path length) and local efficiency (E_l, similar to the clustering coefficient) [16]. For a network G with a set of M nodes $N(G)$,

$$E_g(G) = \frac{1}{M(M-1)} \sum_{j \neq i \in N(G)} \frac{1}{L_{ij}},$$

$$\text{and} \quad E_l(G) = \frac{1}{M} \sum_{i \in N(G)} E_g(G_i),$$

where $L_{i,j}$ corresponds to the path length between nodes i and j, and G_i is the subnetwork composed of the nearest neighbours of i (i.e. the set of nodes directly linked to i). The efficiency measures have been shown to have technical and conceptual advantages over conventional measures such as characteristic path length and clustering coefficient, since it deal with either the disconnected (i.e., consisting of isolated subgraphs) or non-sparse graphs [16]. Typically, a random network is characterized

by a high E_g value and a small E_l value compared with a regular network.

2.4.3. Network topology

The topology of a network can be measured by analyzing the distribution of the node degrees, $p(k)$. The degree k of a node is equal to its total number of connections. Small-world networks can be classified into three categories according to the distribution of their node degrees [15]:

- single-scale networks, the degree distribution of which is exponential, $p(k) = e^{-k/\beta}$;
- scale-free networks, which have a power-law degree distribution, $p(k) = k^{1-\alpha}$;
- broad-scale networks, which are intermediate between the two previous ones with an exponentially truncated power-law distribution of the form $p(k) = e^{-k/\beta}k^{1-\alpha}$;
- where α is the exponent and β the cut-off. Here, the cumulative distribution, $F(k)$, was used to plot the results in order to reduce the effects of noise due to the small set of nodes [19].

2.5. Structure-function comparison

In order to investigate similarities between structural and functional aspects of the full-brain network across subjects, the structural and functional connectivity indices were uniformly thresholded to obtain binary graphs of varying density, or cost, c (i.e., c is the proportion of links that survive the threshold compared to the total number of possible links). All graph theory measures for sCI, fCIr, fCIm, and fCIv were computed for each subject and each cost. To compare graph measures for structural and functional connectivity indices across subjects, we performed an analysis of variance (ANOVA) at a cost of 4% and 6% respectively, with 51 degrees of freedom (4 [connectivity indices] × 13 [subjects] − 1). To select the most appropriate model for the distribution of the node degrees at a given cost, we used the Bayesian information criterion (BIC) [34], which measures the likelihood of the model penalized by its complexity (the lower the BIC value, the more appropriate the model). To assess the goodness-of-fit of the selected model, we used R^2 values for each subject and each connectivity index. An ANOVA was performed to test similarity between model parameters for structural and functional connectivity indices across subjects.

3. Results

A total of 132 nodes, distributed over the whole cortical ($n = 92$) and subcortical ($n = 24$) grey matter and the cerebellum ($n = 16$) were defined among all functional networks identified (Fig. 1). The connectivity matrices in Fig. 2 illustrate the sCI and the fCIr values and the corresponding binary graphs for each pair of nodes for a typical subject. Structural connectivity indices were characterized by sparse matrices (mean: 8.53% and standard deviation [SD]: 1.63% across subjects).

The characteristic path lengths of the networks were close to the values obtained for random networks (Fig. 3, top left). Values of the clustering coefficient C for the connectivity indices were between those corresponding to random and lattice networks (Fig. 3, top right). The C values for the motor and visual tasks were slightly higher than for the rest period, and the C values for the sCI were close to those corresponding to lattice networks. Moreover, the L and C values for functional networks were relatively stable regardless of the experimental condition, and the values corresponding to the sCI were significantly higher than those corresponding to the fCI (ANOVA: $P < 10^{-6}$ at 4% and 6% cost). The scaled L and C values (L_s and C_s) for all the connectivity indices indicated that, independently of the cost, the networks examined here had small-world properties (i.e., $L_s \approx 1$ and $C_s > 1$) (Fig. 3, bottom row). Finally, Fig. 3 highlights the fact that the L_s and C_s values corresponding to the three experimental conditions (fCIr, fCIm, and fCIv) were not significantly different from one another, but significantly lower than those obtained for sCI (ANOVA: $P < 10^{-6}$ at 4% and 6% cost).

In terms of efficiency, the present network analyzed was located between typical random and lattice networks regardless of the connectivity index (Fig. 4). Global efficiencies were close to random values, resulting in a high global efficiency, with significantly lower values for sCI than for fCI (ANOVA: $P < 10^{-3}$ at 4% and 6% cost) (Fig. 4, left). Local efficiencies values were

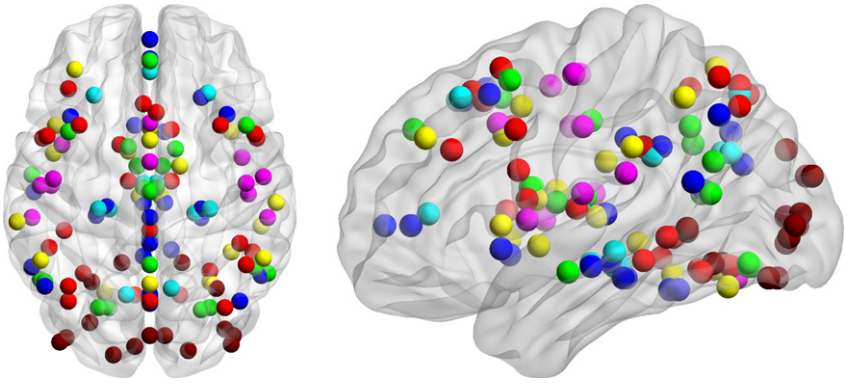

Fig. 1. Regions of interest location in axial (left) and sagittal (right) views superimposed on a brain template surface using the BrainNet Viewer software (www.nitrc.org/projects/bnv). Color codes for group component membership.

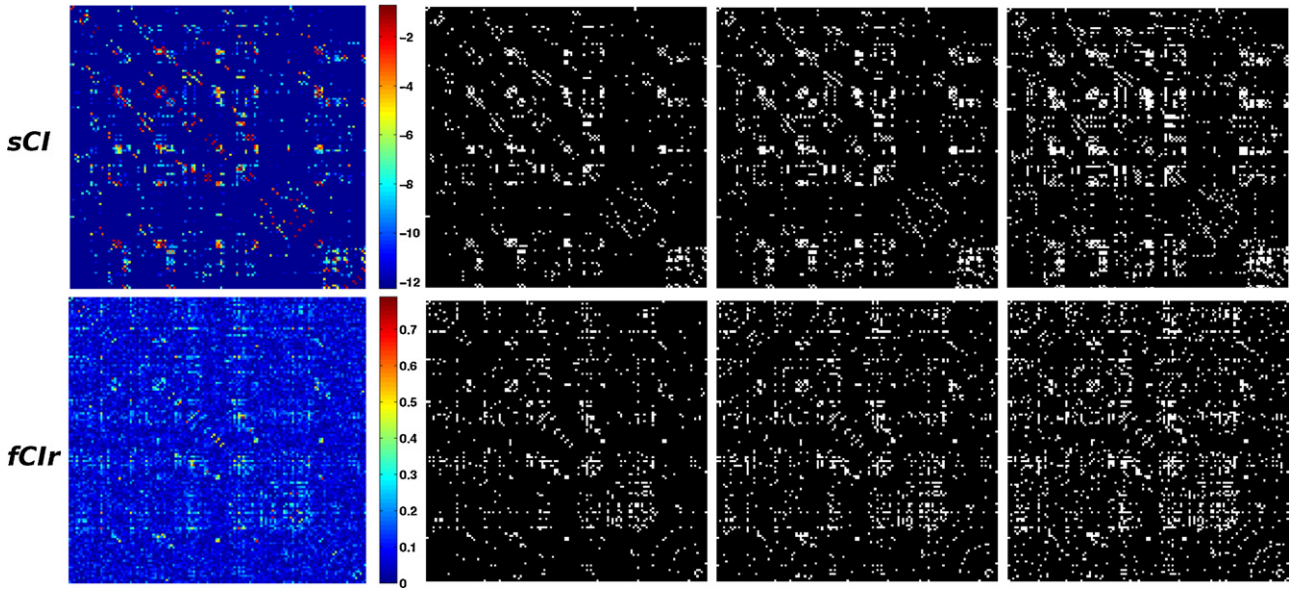

Fig. 2. Connectivity matrices of structural connectivity (top row, left, logarithmic scale) and functional connectivity values at rest (bottom row, left) for one typical subject, and binary matrices resulting from thresholding the connectivity matrices to obtain various cost values (4%, 6%, and 10% cost from columns 2 to 4). Each row and column of the matrices represents a node of the full-brain network.

statistically higher for sCI than for fCI (ANOVA: $P < 10^{-6}$ at 4% and 6% cost) (Fig. 4, right).

In the present study, we found that, according to the BIC, the distributions of the node degrees for sCI and fCI at a cost of 5% were best fitted by the exponentially truncated power-law form (Table 1 and Fig. 5). The fitted distributions did not have significantly different exponents α (ANOVA: $F = 1.85$, $P = 0.15$) and cut-offs β (ANOVA: $F = 2.43$, $P = 0.07$) (Fig. 6) between

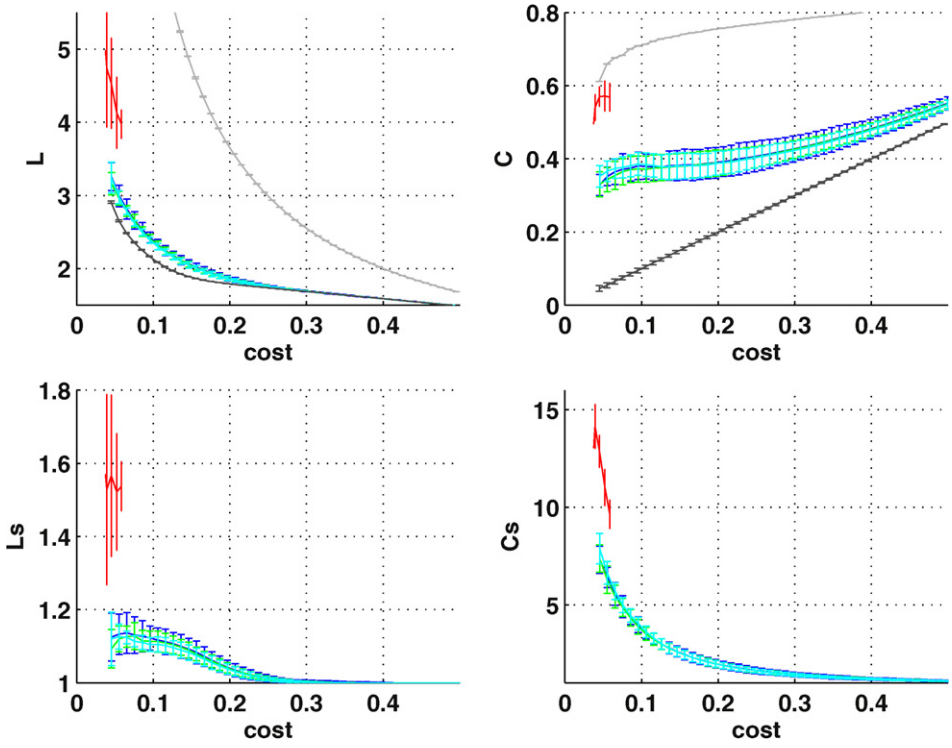

Fig. 3. Mean and standard deviation across subjects of the characteristic path length L (top left), scaled characteristic path length L_s (bottom left), clustering coefficient C (top right), and scaled clustering coefficient C_s (bottom right) as a function of the cost value for structural connectivity (red), functional connectivity et rest (dark blue), functional connectivity during the motor task (green), and functional connectivity for the visual stimulation (light blue), and the corresponding values for typical networks: random (light grey) and lattice (dark grey), with the same size and density as those of the networks analyzed.

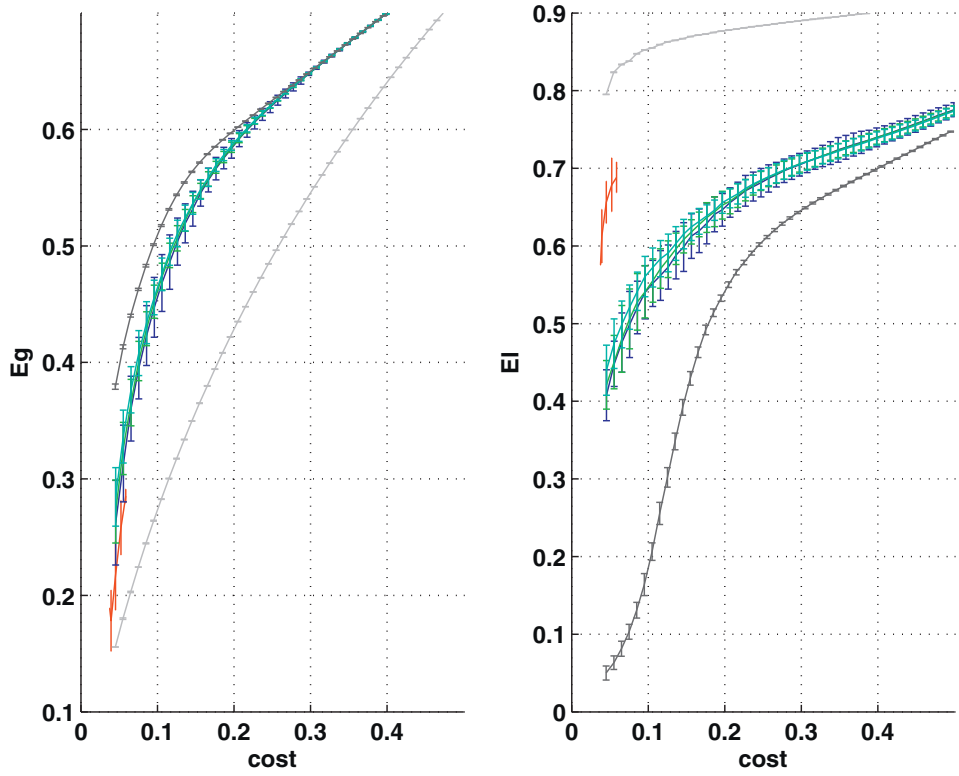

Fig. 4. Mean and standard deviation across subjects of global efficiency (left), and local efficiency (right) for structural connectivity and functional connectivity and corresponding values for random and lattice networks (with the same color code as in Fig. 3).

connectivity indices with, on average, a very good fit ($R^2 = 0.9898$ for sCI; $R^2 = 0.9943$ for fCIr; $R^2 = 0.9942$ for fCIm; and $R^2 = 0.9930$ for fCIv).

4. Discussion

In the present study, we investigated structural and functional connectivity in the human brain using features from graph theory. The nodes of the network were defined using sICA and hierarchical clustering on fMRI data. The structural connectivity index between two nodes was defined as the proportion of fibers that connected these two nodes, while the functional connectivity index between two nodes corresponded to the absolute correlation between the average fMRI time series of these two nodes. These connectivity indices were then thresholded at different costs to produce binary graphs, and graph theory measures were applied to characterize network properties. The results showed that structural and functional connectivity networks shared some important features such as their topology. We also showed that the network functional properties were relatively stable with regard to the experimental protocol (resting-state, motor task or visual task).

One of the key issues regarding the investigation of human brain networks is their definition. Our first step consisted of defining a set of nodes (or ROIs) and then defining the links (or edges) between these nodes. Many approaches may be used to define both the nodes and the links, relying either on structural or functional information, or on other assumptions such as *a priori* atlases. How the definition of the nodes affects the extracted properties is not fully elucidated yet. Wang et al. [35] reported that the network properties, such as the path length, were sensitive to the selected strategy. It has been also suggested that density and degrees distribution are related to the number of node [36]. Here, we defined the nodes of the network from fMRI data at rest, in line with the approach advocated in [37]. The resulting functional networks extracted form a set of distributed areas that reflect the brain's baseline activity. In fact, by definition, ICA component are strongly temporally correlated brain regions, thereby the extracted ROIs are very functionally specific. Besides, data-driven extraction of brain regions allows

Table 1
Mean and standard deviation of the BIC values across subjects, for the three models of the node degree distribution, for sCI and fCI for each task.

	sCI	*fCIr*	*fCIm*	*fCIv*
Truncated power-law	–49.93 ± 4.66	–50.62 ± 7.86	–49.03 ± 5.15	–51.35 ± 9.17
Exponential law	–53.89 ± 4.10	–53.63 ± 5.73	–53.42 ± 3.22	–54.89 ± 6.74
Power-law	–60.27 ± 5.01	–61.60 ± 7.87	–60.66 ± 4.13	–62.72 ± 9.42

sCI: structural connectivity; fCIr: functional connectivity at rest; fCIm: functional connectivity during the motor task; fCIv: functional connectivity for the visual stimulation.

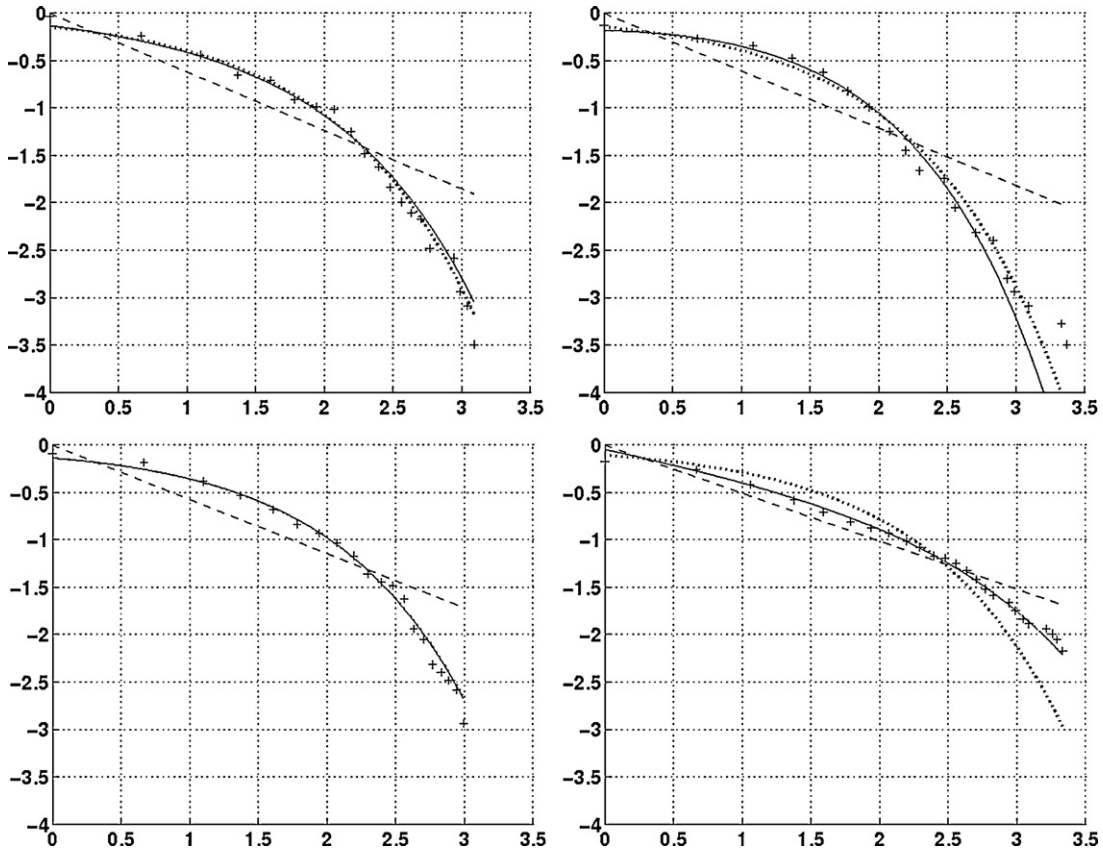

Fig. 5. For the typical subject in Fig. 2, for a cost of 5%, the cumulative distribution $F(k)$ (where k is the degree) of the node degrees according to structural connectivity (sCI, top left), functional connectivity at rest (fCIr, top right), functional connectivity during the motor task (fCIm, bottom left), and functional connectivity for the visual stimulation (fCIv, bottom right). The plus signs represent observed data, the solid line is the fitted exponentially truncated power-law function (Bayesian information criterion [BIC] = –51.46 for sCI; –44.60 for fCIr; –51.22 for fCIm; –70.97 for fCIv), the dashed line the exponential law (BIC = –53.78 for sCI; –48.90 for fCIr; –54.42 for fCIm; –66.57 for fCIv), and the dotted line the power law (BIC = –60.53 for sCI; –56.06 for fCIr; –61.70 for fCIm; –80.71 for fCIv).

for selection of more specific regions, with respect to anatomy, rather than gross anatomical regions, which encompass unrelated functional regions and unreliable fiber tracks. Secondly, the definition of the edges (or connectivity) between nodes is important for the construction of the network. Here, we chose to use classical measures of connectivity, i.e., the fraction of fibers and the absolute correlation between brain nodes. Knowing that the choice of a threshold is still critical [38], the connectivity indices were therefore thresholded uniformly to obtain binary graphs. Then, graph theory measures designed for binary graphs such as the small-world properties were applied [19,20], in order to characterize quantitatively the structural and functional features of the network, each measure being calculated at each cost. The conclusions were similar at various costs.

Previous studies exhibiting graph theory properties of human brain networks have focused on various approaches, such as

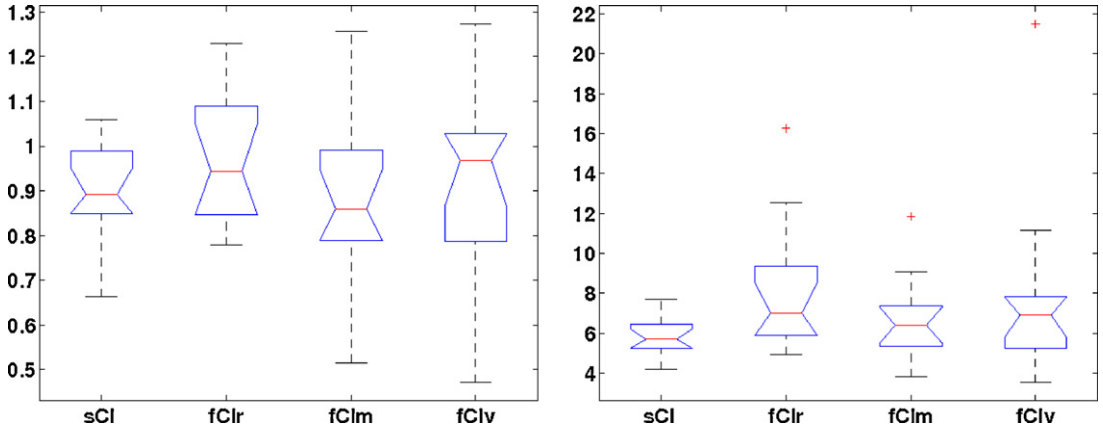

Fig. 6. Boxplot of the exponent α (left) and cut-off β (right) for the fitted exponentially truncated power-law function at 5% cost for the connectivity indices across subjects. For each box, the horizontal lines mark the quartiles, the whiskers extend to the most extreme data points, and outliers are represented by plus signs.

functional imaging [39–42] and structural imaging [39,43–45] with as a common finding the small-world properties of the analyzed networks. Given an *a priori* template of grey matter regions in references [41] and [39], the authors applied partial correlation and a discrete wavelet transform, respectively, to fMRI time series at rest to estimate functional connectivity and found a small-world topology of sparse connections. The first study showing the small-world properties of human brain structural networks was initiated by He et al. [45], the graph was built based on the correlation between the cortical thicknesses of brain areas, assuming that the strength of the links between brain regions (or structural pattern) could be related to the cross-correlation of cortical thickness. More recently, in references [43] and [44], maps of about 80 cortical and subcortical grey matter regions were constructed from DWI data and analyzed using graph theory. Networks exhibited the small-world properties and some regions like the precuneus and the superior frontal and parietal cortices were found to be network hubs [46]. Node topology, as measured by the distribution of the node degrees, presents also consistent characteristics in the literature with the main observation of broad-scale topology [6,39,43,45], despite a controversial result in reference [47] showing a scale-free topology. To our knowledge, only one study investigated the graph properties in both structural and functional connectivity [48]. The authors derived a group-level network and investigated its properties using both structural and functional connectivity. However, the analyzed network was defined with an arbitrary template and no statistical test was used to quantify to which extent both representations (structural and functional) were related.

Our results are in agreement with those of previous investigators, in that we observed small-world properties and broad-scale topology with both structural and functional connectivity for the same subjects. This observation demonstrates that structure shares common properties with function. Some of our results were similar to those obtained in reference [48]. Nevertheless, here we assessed network properties from the same subjects in various states (at rest, during a motor task, and visual stimulation). Besides, we observed that functional network properties were relatively stable with regard to the experimental protocol (resting-state, motor task or visual task). This contradicts previous results [47], where it was observed some variations in the distribution of the node degrees during a finger-tapping task and listening to music using fMRI data. Our results rather suggest that the intrinsic functional properties of the network were stable with regard to the task. The possible functional reorganisation during a specific task might imply only local changes in the network properties. Another implication to this for future research is that it is possible to look into subnetworks of graphs generated from different functional states to reveal insights into what properties are changing at a region-by-region level.

The main features of the small-world properties correspond to the two essential organizational principles of the human brain [38]. The first one is integration, corresponding to the coordination of distributed resources to create coherent states, which can be related to the characteristic path length or the global efficiency. The second one is segregation, meaning a rapid extraction of information, measured by local clustering or local efficiency. Another important property of a network is its node topology, which can be described by the distribution of node degrees [15]. The network's node topology measures graph behaviour, such as resilience to attacks [39].

Showing some similarities between structural and functional features tends, in turn, to suggest that structure is linked to function. Another important question that emerges from this observation is how to relate structure to function. Few studies have addressed the direct link between structural connectivity networks (i.e., networks as defined by DWI) and functional connectivity networks (i.e., networks as defined by fMRI). Some of the studies that examined the anatomical substrate of specific functional regions such as the primary motor cortex [49] or the visual system [23] suggested that structure and function as measured by MRI can be linked together. However, such investigations remain limited due to the complexity of the human brain, as well as the inability of these approaches to examine networks rather than regions. Indeed, networks involve a large number of regions forming a complex architecture with specific properties that cannot be described locally [38,50]. More recently, some studies demonstrated that specific functional brain networks extracted at rest such as the default-mode network [51] or the attentional and motor networks [52] were anatomically connected. However, an anatomical link between functional regions does not necessarily imply a functional connection between these regions and vice versa, due particularly to indirect connections. Furthermore, these studies only provided visual evidence in favor of a relationship between structure and function. It is still unclear in what measure structure supports function; especially whether structural features of brain networks serve as a substrate to the functional features. A recent study investigated the functional processes underlying the structure using a neural mass to model the functional activity, the resulting simulated functional connectivity was statistically correlated with the resting-state fMRI derived functional connectivity [53].

In reference [44], the structural network was revealed by using hard angular resolution diffusion imaging, which deals with the complexity of diffusion distribution in some voxels [4,5,54] using new diffusion models and tractography methods [31,54,55]. Yet, in this work, we used a standard clinical sequence (with 12 diffusion-weighted directions) that allows one to extract a simple diffusion model like the diffusion tensor, which models the local diffusion by an ellipsoid, but does not solve fiber crossing issues. The influence of the diffusion model on structural connectivity measures is still an open issue. For function, many approaches exist to quantify links between distinct brain regions from functional imaging, as partial correlation or wavelet transformation [39,41]. As for structural connectivity, the effect of a functional interaction measure on network properties is unknown. It would be of great interest to investigate multimodal MRI network properties using different imaging sequences and preprocessing steps, and several interaction measures.

5. Conclusion

Our results suggest the existence of a relationship characterized by graph theory measures between functional behavior and the underlying structure of human brain networks. Probabilistic tracking accurately described structural connectivity, yielding a structural index that proved to have similar properties to functional connectivity. Such a conclusion is in agreement with the recent literature, which indeed suggests that functional organization of the brain is embedded within some structural organization.

Acknowledgments

The authors would like to thank S. Jbabdi (Oxford Centre for Functional Magnetic Resonance Imaging of the Brain, FMRIB, University of Oxford) for insightful discussions about this work.

References

[1] Varela F, Lachaux J, Rodriguez E, Martinerie J. The brainweb: phase synchronization and large-scale integration. Nat Rev Neurosci 2001;2:229–39.
[2] Luria AR. The functional organization of the brain. Sci Am 1970;222:66–72.
[3] Mesulam MM. From sensation to cognition. Brain 1998;121:1013–52.
[4] Mori S, Zhang J. Principles of diffusion tensor imaging and its applications to basic neuroscience research. Neuron 2006;51:527–39.
[5] Hagmann P, Kurant M, Gigandet X, Thiran P, Weeden VJ, Meuli R, et al. Mapping human whole-brain structural networks with diffusion MRI. PLoS One 2007;2:e597.
[6] Iturria-Medina Y, Canales-Rodríguez E, Melie-García L, Valdés-Hernández P, Martínez-Montes E, Alemán-Gómez Y, et al. Characterizing brain anatomical connections using diffusion weighted MRI and graph theory. Neuroimage 2007;36:645–60.
[7] Logothetis NK, Pauls J, Augath M, Trinath T, Oeltermann A. Neurophysiological investigation of the basis of the fMRI signal. Nature 2001;412:150–7.
[8] Raichle M, Mintun M. Brain work and brain imaging. Ann Rev Neurosci 2006;29:449–76.
[9] Beckmann CF, Smith SM. Tensorial extensions of independent component analysis for multisubject fMRI analysis. Neuroimage 2005;25:294–311.
[10] Beckmann CF, De Luca M, Devlin JT, Smith SM. Investigations into resting-state connectivity using independent component analysis. Philos Trans R Soc 2005;360:1001–13.
[11] Damoiseaux JS, Rombouts SARB, Barkhof F, Scheltens PC, Stam J, Smith SM, et al. Consistent resting-state networks across healthy subjects. Proc Natl Acad Sci U S A 2006;103(37):13848–53.
[12] De Luca M, Beckmann CF, De Stefano N, Matthews PM, Smith SM. fMRI resting state networks define distinct modes of long-distance interactions in the human brain. Neuroimage 2006;29:1359–67.
[13] Esposito F, Scarabino T, Hyvarinen A, Himberg J, Formisano E, Comani S, et al. Independent component analysis of fMRI group studies by self-organizing clustering. Neuroimage 2005;25:193–205.
[14] Perlbarg V, Marrelec G. Contribution of exploratory methods to the investigation of extended large-scale brain networks in functional MRI: methodologies, results, and challenges. Int J Biomed Imaging 2008;2008:218519.
[15] Amaral LA, Scala A, Barthélémy M, Stanley HE. Classes of small-world networks. Proc Natl Acad Sci U S A 2000;97:11149–52.
[16] Latora V, Marchiori M. Efficient behavior of small-world networks. Phys Rev Lett 2001;87:198701–4.
[17] Newman MEJ. The structure and function of complex networks. SIAM Rev 2003;45:167–256.
[18] Ravasz E, Barabási AL. Hierarchical organization in complex networks. Phys Rev E 2003;67:026112.
[19] Strogatz SH. Exploring complex networks. Nature 2001;410:268–76.
[20] Watts DJ, Strogatz SH. Collective dynamics of "small-world" networks. Nature 1998;393:440–2.
[21] Reijneveld JC, Ponten SC, Berendse HW, Stam CJ. The application of graph theoretical analysis to complex networks in the brain. Clin Neurophysiol 2007;118:2317–31.
[22] Sporns O, Tononi G, Edelman G. Theoretical neuroanatomy and the connectivity of the cerebral cortex. Behav Brain Res 2002;135:69–74.
[23] Sporns O, Chialvo D, Kaiser M, Hilgetag C. Organization, development and function of complex brain networks. Trends Cogn Sci 2004;8:418–25.
[24] Ashburner J, Friston K. Nonlinear spatial normalization using basis functions. Hum Brain Mapp 1999;7:254–66.
[25] Jenkinson M, Smith S. A global optimisation method for robust affine registration of brain images. Med Image Anal 2001;5:143–56.
[26] Smith SM. Fast robust automated brain extraction. Hum Brain Mapp 2002;17:143–55.
[27] McKeown M, Makeig S, Brown G, Jung T, Kindermann S, Bell A, et al. Analysis of fMRI data by blind separation into independent spatial components. Hum Brain Mapp 1998;6:160–88.
[28] Perlbarg V, Marrelec G, Doyon J, Pélégrini-Issac M, Lehéricy S, Benali H. NEDICA: detection of group functional networks in fMRI using spatial independent component analysis. Proceedings of the 2008 IEEE International Symposium on Biomedical Imaging: From Nano to Macro (ISBI'08); 2008, p. 1247–50.
[29] Hartigan JA. Clustering Algorithms. John Wiley and Sons Inc (Ed.); 1975.
[30] Perlbarg V, Bellec P, Anton J, Pélégrini-Issac M, Doyon J, Benali H. CORSICA: correction of structured noise in fMRI by automatic identification of ICA components. Magn Reson Imaging 2007;25:35–46.
[31] Behrens TEJ, Johansen-Berg H, Jbabdi S, Rushworth MFS, Woolrich MW. Probabilistic diffusion tractography with multiple fibre orientations: what can we gain? Neuroimage 2007;34:144–55.
[32] Maslov S, Sneppen K. Specificity and stability in topology of protein networks. Science 2002;296:910–3.
[33] Sporns O, Zwi JD. The small world of the cerebral cortex. Neuroinformatics 2004;2:145–62.
[34] Schwarz G. Estimating the dimension of a model. Ann Stat 1978;6:461–4.
[35] Wang J, Wang L, Zang Y, Yang H, Tang H, Gong Q, et al. Parcellation-dependent small-world brain functional networks: a resting-state fMRI study. Hum Brain Mapp 2009;30:1511–23.
[36] Zalesky A, Fornito A, Harding IH, Cocchi L, Yucel M, Pantelis C, et al. Whole-brain anatomical netorks: does the choice of nodes matter? Neuroimage 2010;50:970–83.
[37] Smith S. The future of FMRI connectivity. Neuroimage 2012, http://dx.doi.org/10.1016/j.neuroimage.2012.01.022.
[38] Bullmore E, Sporns O. Complex brain networks: graph theoretical analysis of structural and functional systems. Nat Rev Neurosci 2009;10:186–98.
[39] Achard S, Salvador R, Whitcher B, Suckling J, Bullmore E. A resilient, low-frequency, small-world human brain functional network with highly connected association cortical hubs. J Neurosci 2006;26:63–72.
[40] Micheloyannis S, Pachou E, Stam C, Vourkas M, Erimaki S, Tsirka V. Using graph theoretical analysis of multi channel EEG to evaluate the neural efficiency hypothesis. Neurosci Lett 2006;402:273–7.
[41] Salvador R, Suckling J, Coleman M, Pickard J, Menon D, Bullmore E. Neurophysiological architecture of functional magnetic resonance images of human brain. Cereb Cortex 2005;15:1332–42.
[42] Stam CJ. Functional connectivity patterns of human magnetoencephalographic recordings: a "small-world" network? Neurosci Lett 2004;355:25–8.
[43] Gong G, He Y, Concha L, Lebel C, Gross D, Evans A, et al. Mapping anatomical connectivity patterns of human cerebral cortex using in vivo diffusion tensor imaging tractography. Cereb Cortex 2009;19:524–36.
[44] Hagmann P, Cammoun L, Gigandet X, Meuli R, Honey C, Wedeen V, et al. Mapping the structural core of human cerebral cortex. PLoS Biol 2008;6:e159.

[45] He Y, Chen ZJ, Evans AC. Small-world anatomical networks in the human brain revealed by cortical thickness from MRI. Cereb Cortex 2007;10:2407–19.
[46] Sporns O, Honey C, Kötter R. Identification and classification of hubs in brain networks. PLoS One 2007;2:e1049.
[47] Eguíluz V, Chialvo D, Cecchi G, Baliki M, Apkarian A. Scale-free brain functional networks. Phys Rev Lett 2005;94:018102.
[48] Park C, Kim SY, Kim Y, Kim K. Comparison of the small-world topology between anatomical and functional connectivity in the human brain. Physica A 2008;387:5958–62.
[49] Guye M, Parker GJM, Symms M, Boulby P, Barker GJ, Duncana JS. Combined functional MRI and tractography to demonstrate the connectivity of the human primary motor cortex in vivo. Neuroimage 2003;19:1349–60.
[50] Toosy A, Ciccarelli O, Parker G, Wheeler-Kingshott C, Miller D, Thompson A. Characterizing function-structure relationships in the human visual system with functional MRI and diffusion tensor imaging. Neuroimage 2004;21:1452–63.
[51] Greicius MD, Supekar K, Menon V, Dougherty RF. Resting-state functional connectivity reflects structural connectivity in the default mode network. Cereb Cortex 2009;19(1):72–8.
[52] Van Den Heuvel MP, Mandl RCW, Kahn RS, Hulshoff Pol HE. Functionally linked resting-state networks reflect the underlying structural connectivity architecture of the human brain. Hum Brain Mapp 2009;30:3127–41.
[53] Honey C, Sporns O, Cammoun L, Gigandet X, Thiran J, Meuli R, et al. Predicting human resting-state functional connectivity from structural connectivity. Proc Natl Acad Sci U S A 2009;106:2035–40.
[54] Tuch D, Reese T, Wiegell M, Makris N, Belliveau J, Wedeen V. High angular resolution diffusion imaging reveals intravoxel white matter fiber heterogeneity. Magn Reson Med 2002;48:577–82.
[55] Descoteaux M, Deriche R, Knosche TR, Anwander A. Deterministic and probabilistic tractography based on complex fibre orientation distributions. IEEE Trans Med Imaging 2009;28:269–86.